General Disclaimer

One or more of the Following Statements may affect this Document

- This document has been reproduced from the best copy furnished by the organizational source. It is being released in the interest of making available as much information as possible.

- This document may contain data, which exceeds the sheet parameters. It was furnished in this condition by the organizational source and is the best copy available.

- This document may contain tone-on-tone or color graphs, charts and/or pictures, which have been reproduced in black and white.

- This document is paginated as submitted by the original source.

- Portions of this document are not fully legible due to the historical nature of some of the material. However, it is the best reproduction available from the original submission.

NASA Technical Memorandum 73297

A Fourier Transform Spectrometer for Visible and Near-Ultraviolet Measurements of Atmospheric Absorption

C. L. Parsons
J. C. Gerlach
and
M. Whitehurst

June 1982

National Aeronautics and Space Administration

Goddard Space Flight Center
Wallops Flight Center
Wallops Island, Virginia 23337

NASA Technical Memorandum 73297

A Fourier Transform Spectrometer for Visible and Near-Ultraviolet Measurements of Atmospheric Absorption

C. L. Parsons and J. C. Gerlach

NASA Goddard Space Flight Center
Wallops Flight Center
Wallops Island, Virginia 23337

and

M. Whitehurst

Joule' Corporation
P.O. Box 21
Wallops Island, Virginia 23337

National Aeronautics and
Space Administration

Goddard Space Flight Center
Wallops Flight Center
Wallops Island, Virginia 23337

A FOURIER TRANSFORM SPECTROMETER FOR VISIBLE AND NEAR-ULTRAVIOLET MEASUREMENTS OF ATMOSPHERIC ABSORPTION

C. L. Parsons
J. C. Gerlach
NASA Goddard Space Flight Center
Wallops Flight Center
Wallops Island, VA 23337

and

M. Whitehurst
Joule Corporation
Wallops Island, VA 23337

ABSTRACT

The development of a prototype, ground-based, sun-pointed Michelson interferometric spectrometer is described. Its intended use is to measure the atmospheric amount of various gases which absorb in the near-infrared, visible, and near-ultraviolet portions of the electromagnetic spectrum. Preliminary spectra which contain the a, 0.8 μm, and ρστ water vapor absorption bands in the near-infrared are presented to indicate the present capability of the system. Ultimately, the spectrometer will be used to explore the feasible applications of Fourier transform spectroscopy in the ultraviolet where grating spectrometers have been exclusively used previously.

INTRODUCTION

A recent paper by Baker et al. (1981) describes first the historical development of Michelson interferometry until it reached maturity in the 1950's. Then the emphasis is centered on the sub-discipline of high-altitude atmospheric emission spectroscopy using infrared Fourier transform spectroscopy (FTS) during the past two decades. The well-known attributes of Fourier transform spectroscopy, namely the spectral multiplex advantage and greater throughput, are distinct advantages in the infrared. The reader is

referred to Chamberlain (1979), Vanasse (1977, 1981), and Vanasse et al. (1971) for comprehensive reviews of the FTS technique and its traditional applications. Quite recently, some work has been started in FTS applications in the visible wavelengths (Elsworth et al., 1974; Elsworth et al., 1980). These studies have involved developing instrumentation for obtaining spectra of the airglow. In this paper, a prototype instrument is described that is intended for use in measuring the concentration of various atmospheric absorbing gases using the differential absorption technique and with the sun as the optical source. Ultimately, the feasibility of using the FTS technique at wavelengths as low as 3000Å will be examined with this system.

Several constituents have already been measured in the visible and ultraviolet using the differential absorption technique with dispersive optical instrumentation. The Dobson spectrophotometer, a double prism spectrometer, the Brewer grating spectrometer, and several filter photometer systems use discrete lines in the Hartley-Huggins bands between 3000 and 3400Å to infer the atmospheric ozone content (Parsons et al., 1982). The former instrument is the primary ground-based detector of the total ozone amount and is used throughout a network of ozone monitoring stations around the world. The Brewer spectrometer (Brewer, 1973; Brewer and Kerr, 1973) uses five lines that differ somewhat from those utilized by Dobson (1931) and which were selected to minimize the influence of sulphur dioxide on the ozone measurements. Furthermore, the Brewer instrument uses new technology and automatic data processing in an effort to compete favorably with the established Dobson. Garrison et al. (1979) have espoused the importance of making multiwavelength measurements in the ultraviolet region and a least squares method to compute the total ozone thickness to achieve higher accuracy.

McMahon and Simmons (1980) and Noxon (1975) have used differential optical absorption to measure NO_2, Noxon et al. (1978) have measured NO_3 and Platt and colleagues have measured various constituents including CH_2O, HNO_2, O_3, NO_2, NO_3, and SO_2 (Platt and Perner, 1980; Platt et al., 1980a; Platt et al., 1979; Platt et al., 1980b). This recapitulation is not intended to be all-inclusive but is meant to indicate the current interest in the differential optical absorption technique in the visible and ultraviolet. The FTS system described in this paper may have an application in the measurement of all of these constituents because of its inherent flexibility. This report documents the system's development thus far and highlights the improvements that will be necessary if its intended use is to be realized.

THEORY

In the Michelson interferometer, incoming light is divided by a beamsplitter into two components of nominally equal intensity which are passed through two arms, one of which is fixed in optical length and one which is variable. The optical path difference, x, is the difference of the two lengths. If the signal component coming from the fixed arm is given by E(t) and the signal component from the variable length arm is $E(t-\tau)$ where τ is the time difference due to the path difference x, then the recombined signal observed by the detector is

$$\overline{D(x,t)} = \langle [E(t) + E(t-\tau)]^2 \rangle \qquad (1)$$

where the bar indicates an average over a statistically fluctuating variable and

$$\langle (\quad) \rangle = \frac{1}{T} \int_{t-T/2}^{t+T/2} (\quad) \, dt$$

Expanding (1),

$$D(x,t) = \langle E^2(t) \rangle + \langle E^2(t-\tau) \rangle + 2\langle E(t)E(t-\tau) \rangle$$

If the source intensity I_0 is constant during the measurement and if the beamsplitter does indeed divide the signal into two equal components,

$$\langle E^2(t) \rangle = \frac{I_0}{2} = \langle E^2(t-\tau) \rangle \qquad (2)$$

then,

$$\overline{D(x,t)} = I_0 + 2\langle E(t)E(t-\tau) \rangle$$

Using (2),

$$D(x,t) = I_0 \left(1 + \frac{\langle E(t)E(t-\tau) \rangle}{\langle E^2(t) \rangle} \right) \qquad (3)$$

That is, the observed recombined signal consists of a constant component and an oscillating component that depends upon τ, or equivalently x. From the Wiener-Khintchine theorem (see, e.g., Klein, 1970, p. 239), the oscillating term, the normalized autocorrelation function of the signal E(t), can be equated to the cosine Fourier transform of the signal's spectral distribution function, $P(\sigma)$. That is,

$$\gamma(\tau) = \frac{\langle E(t)E(t-\tau)\rangle}{\langle E^2(t)\rangle} = \int_0^\infty P(\nu)\cos 2\pi\nu\tau d\nu \qquad (4)$$

A change of variables is convenient in Fourier transform spectroscopy, so the transform relationship used hereafter is

$$\gamma(x) = \int_0^\infty P(\sigma)\cos 2\pi\sigma x d\sigma \qquad (5)$$

where $\gamma(x)$ is the interferogram and $P(\sigma)$ is the wavenumber spectrum that is to be recovered from $\gamma(x)$. The major function of the FTS system to be described is therefore to produce a recording of $\gamma(x)$ that is as pure as possible. An inverse Fourier transform process then produces the original spectrum $P(\sigma)$ that created the interferogram.

In (5), a one-sided transform is indicated. In Chamberlain (1979), a detailed discussion of the advantages and disadvantages of one and two-sided transformations can be found. Essentially, the two-sided version minimizes the importance of phase errors that can be contributed to $\gamma(x)$ from a variety of causes at the expense of the additional calculations needed for the second side. Because this prototype system is intended for use at small wavelengths where the phase errors are more difficult to eliminate, the two-sided transform pair relationship is adapted in this paper. That is,

$$\gamma(x) = \int_{-\infty}^\infty P(\sigma)e^{2\pi i\sigma x} d\sigma \qquad (6)$$

Of course, the interference pattern is complicated making the inversion of (6) impossible in closed form. Instead it is performed numerically using a Fast Fourier Transform (FFT) algorithm that will be described later in detail. One consequence of the discrete, finite approach is that the limits of (6) must be finite. The maximum wavenumber, σ_{max}, that is handled by the FFT is the parameter from which the other characteristics of the numerical transform process can be deduced. From the Nyquist sampling condition, the resolution in the path difference domain, Δx, can be found from

$$\Delta x \leq \frac{1}{2\sigma_{max}} \qquad (7)$$

The total path difference X_T is then

$$X_T = N \cdot \Delta x \qquad (8)$$

where N is the number of discrete samples in the interferogram. The wavenumber domain resolution, $\Delta\sigma$, can be computed using (7) and (8) and found to be

$$\Delta\sigma = \frac{2\,\sigma_{max}}{N} = \frac{2}{N} \cdot \frac{1}{2\Delta x} = \frac{1}{x_T} \qquad (9)$$

Equations (7), (8), and (9) characterize the numerical transform process. An excellent discussion of the FFT and its applications is found in Brigham (1974).

DESCRIPTION OF THE OPTICAL DESIGN

The optical design used for this FTS system is that of Sternberg and James (1964). It has the distinct advantage that the parallel motion necessary in the movement of one mirror in a traditional Michelson interferometer is replaced by a single rotation. Figure 1 illustrates the design. The beamsplitter and a compensator plate are colocated at the axis of rotation. The moveable plate also contains two front-surface mirrors oriented to be parallel to the beamsplitter and at 45° to the incoming light. The light reflected by the beamsplitter strikes the 45° mirror in its path, is directed to a stationary mirror oriented perpendicular to its direction, and is returned along the same path. The incident light that is transmitted by the beamsplitter strikes the other stationary, perpendicular mirror and is reflected back to the beamsplitter. When the positions of the stationary mirrors are fixed such that the path differences traced by the two component beams are the same at the particular orientation of the moveable plate, then the two beams are recombined constructively at the beamsplitter. This alignment will be referred to as the zero path difference (ZPD) position. As the plate is rotated through an angle θ, the path difference, as shown by Sternberg and James (1964), can be calculated from the trigonometric relationship

$$x = 2H \left\{ \sin (45° + \theta) - 1/\sqrt{2} \right\} \qquad (10)$$

This design is relatively insensitive to vibrations and as pointed out by Sternberg and James (1964), this interferometer's alignment is not affected by either a translation without rotation or by a rotation about any axis. A rotation will change the path difference traced by the two component beams but if an independent measurement of x is made, this is not consequential. The costs incurred by adopting this design are the expenses of an additional precision front surface mirror and of larger sized optics. The latter requirement results from the movement of the light beams across the optics during rotation of the plate.

The optics used in this prototype instrument have the following specifications. The beamsplitter is a 2-1/4" diameter plate of 1/2" thick fused silica with an overcoat of

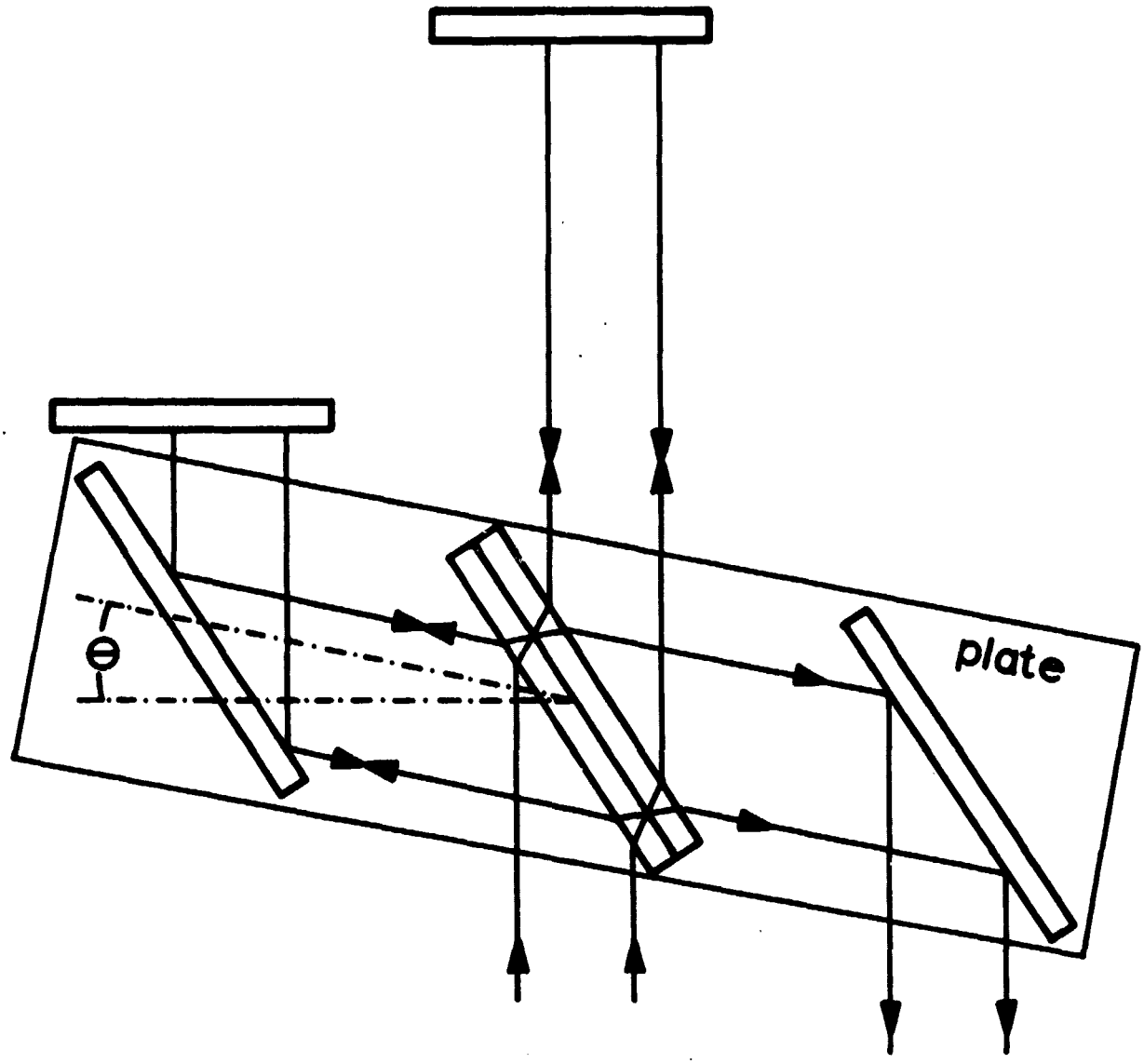

Figure 1. The modified Michelson interferometer optical design of Sternberg and James (1964) used in the Wallops Fourier Transform Spectrometer.

magnesium fluoride. Its sides are parallel to within one arc second and it is flat to 1/20 wavelength at 5890Å. The compensator plate is of the same dimensions. It is coated with a single layer of anti-reflective material that is optimized for the wavelength range of 2500-3000Å; the coating's thickness matches the thickness of the beamsplitter's coating. All mirrors are front-surface mirrors, flat to 1/40 wavelength at 5890Å and are circular with a diameter of 2-1/4".

SYSTEM DESCRIPTION

Figure 2 shows the prototype instrument system broken into components for descriptive purposes. Two light sources illuminate tne modified Michelson interferometer. The first, the sun, is the source that contains the spectral information of interest. The second is a Helium-Neon 5 mw laser that is used to independently determine the path difference in the optics at a particular angle of rotation θ. The laser is, of course, coherent and, when adjusted properly, in collimation. The sun's beam is directed into the Michelson beamsplitter from a heliostat and it is of course in good collimation as well. Baffles ensure that little light from one beam contaminates the other. There is no aperture or slit necessary but two additional optical elements are used at the front end of the optics. One is a filter which can be used to cut down on the width of the spectrum of the solar beam entering the interferometer. If high resolution work is required and the number of samples to be processed is limited by a system constraint, this component becomes a firm requirement.

The other component, which is an absolute requirement, is a polarizer. Fresnel's formulas for reflectance state that for an incident electric field vector which is parallel to the plane of incidence, the reflectance, r, is given by

$$r_{\parallel} = \frac{\tan^2(\phi-\phi')}{\tan^2(\phi+\phi')} \tag{11}$$

where ϕ and ϕ' are the angles of incidence and refraction, respectively. For a perpendicular electric field vector,

$$r_{\perp} = \frac{\sin^2(\phi-\phi')}{\sin^2(\phi+\phi')} \tag{12}$$

Natural light contains equal portions of the two field orientations so that

$$r_{natural} = \frac{1}{2}\,\frac{\tan^2(\phi-\phi')}{\tan^2(\phi+\phi')} + \frac{1}{2}\,\frac{\sin^2(\phi-\phi')}{\sin^2(\phi+\phi')} \tag{13}$$

Without a polarizer in front, natural light enters the interferometer. At the front surface of the beamsplitter, reflection occurs according to (13). For a 45° orientation, about 5% of the incident light is reflected. This 5% is then free to interfere construc-

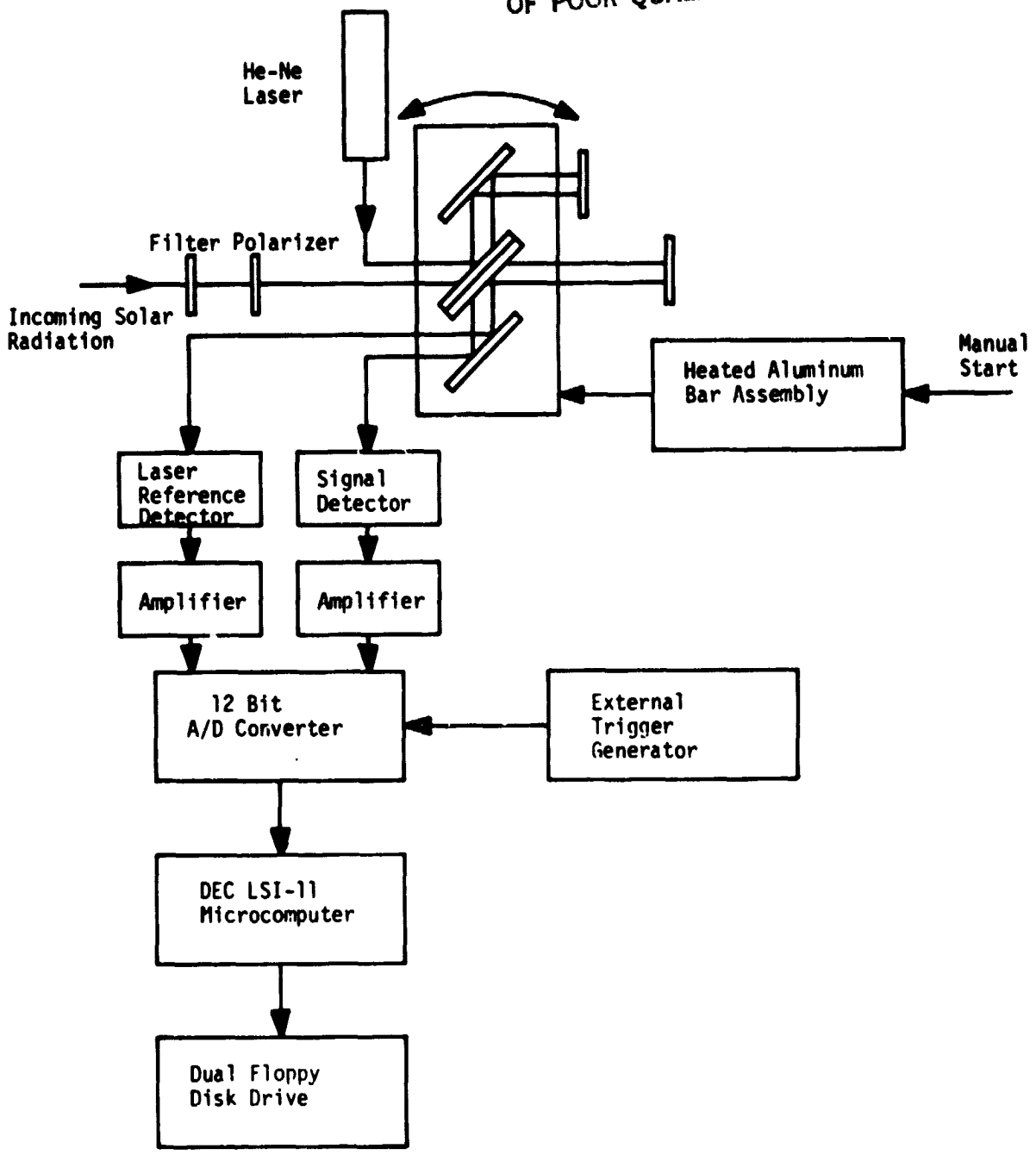

Figure 2. The current configuration of the prototype interferometric spectrometer in schematic form.

tively and destructively with the beams in the two arms of the interferometer. When these are recombined, the initially reflected light severely degrades the resulting interferogram. By using a polarizer, the perpendicular orientation of the electric field vector of the incoming light can be blocked. Only .85% of the parallel component is reflected at 45° so the problem is greatly reduced.

After exiting from the interferometer, the recombined laser and sunlight beams are directed onto silicon photodiode detectors. Currently, the sun-signal is detected with a UDT-500 UV unit and the laser signal with a UDT PIN-SPOT/2D detector. Because of the high energy content of the solar and laser beams, a great deal of amplification is not needed, but some amplification is produced with integrated circuit operational amplifiers. The amount is adjustable and serves mainly to keep the detected signal levels within a range that is compatible with the automatic data processing requirements. The variability of the solar flux at the ground resulting from atmospheric haze, clouds, the time of day, and the day of the year is accounted for in this way.

After formatting, the two signals are transmitted to an analog-to-digital converter that samples them at prescribed time intervals set by an external pulse generator. The 16-channel A/D unit has 12 bit resolution and a throughput speed of 35 KHz. The digitized signals are then stored in buffers in a computer for subsequent processing. A dedicated DEC LSI-11 microcomputer with a dual floppy disk drive is used presently for controlling the A/D conversion and for performing the FFT and other required data manipulations.

The last component of the system configuration shown in Figure 2 is the heated bar assembly used to cause the rotation of the plate in the interferometer. An aluminum cylindrical rod about 5" in length is wrapped with a Nichrome heating coil. A Variac is used to supply an AC voltage across the coil. By varying the voltage, the rate of linear expansion of the rod can be controlled. With a coefficient of linear expansion of $2.4 \cdot 10^{-5}$ $°C^{-1}$, aluminum is inexpensive, readily available and has a range of expansion that is well-matched to the range of movement needed for the interferometer.

Figure 3 shows a portion of the interferograms for the solar and laser signals as an example of the instrument's operation. The actual segments shown are centered around ZPD. The ordinates are voltages and the abscissa is time. Each sample shown is the value seized by the A/D converter when triggered by the external pulse generator. For this example, the intersample spacing is 20 msec. The laser, a coherent and nearly monochromatic source, produces a fringe pattern that is essentially independent of path difference so that the envelope of the laser interferogram does not decay as x grows away from ZPD. The solar signal, being broad-banded, has a much shorter coherence length so its envelope does decrease for x away from ZPD. The monochromatic characteristic of the laser signal is exploited to produce the independent determination of path difference needed to perform the inverse FFT. Instead of samples as a function of time, sampling is

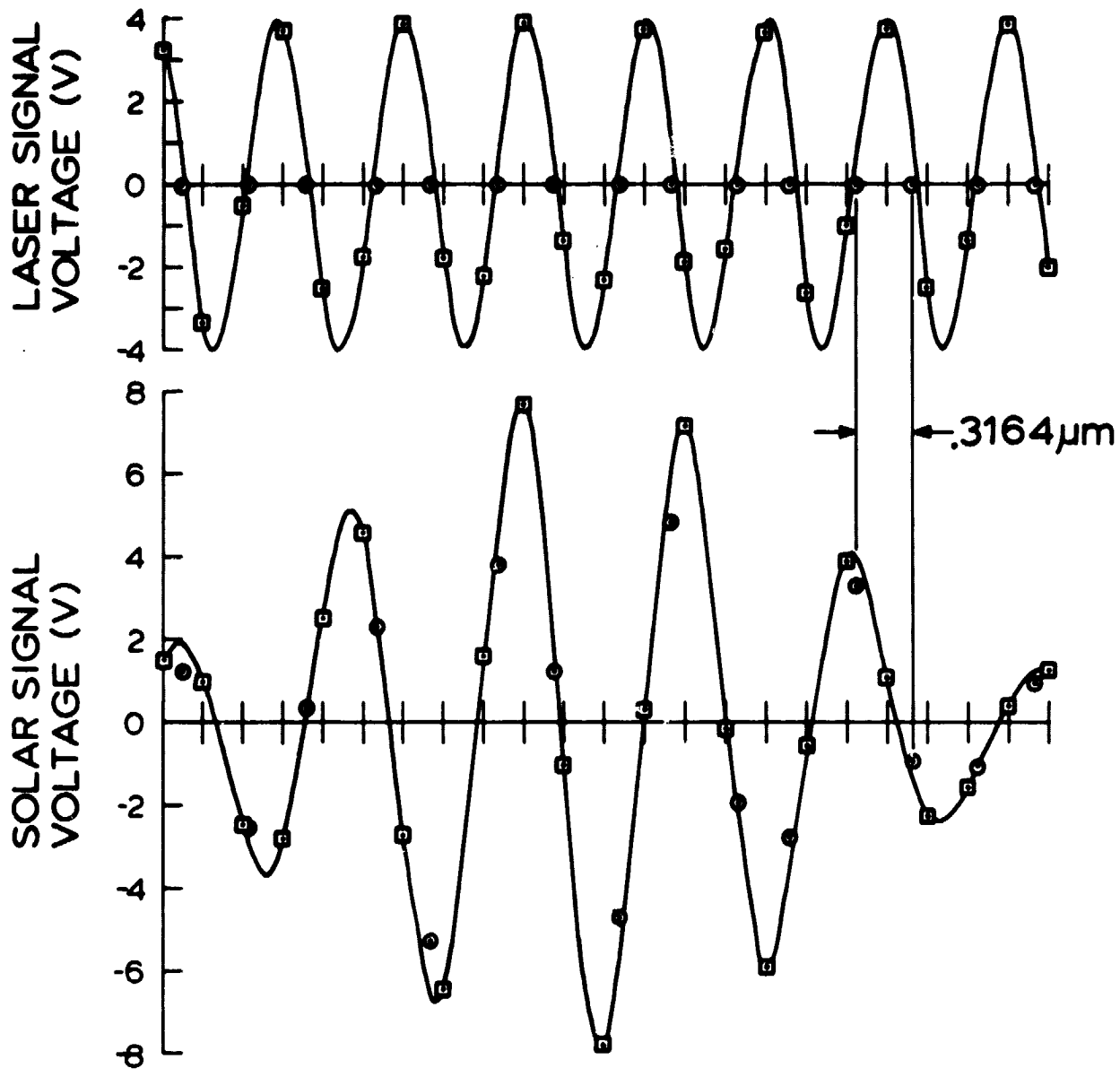

Figure 3. The center of representative laser reference and solar signal interferograms. The squares indicate samples equally spaced in time resulting from triggering by an external pulse generator. The circles are samples approximately equally spaced in path difference as computed by linear interpolation of the constant time samples.

desired at fixed intervals of x. Because the laser wavelength is 6328Å, a complete cycle in the laser interferogram must indicate that the path difference has changed by .6328 μm. Therefore, after digitization and buffering, the laser signal is processed through an algorithm that uses the pulse generator triggered samples and a linear interpolator to determine the location in time of the zero-crossing points. These are indicated in Figure 3 as well, and are used with a linear interpolator to determine approximate values of the solar signal at the zero-crossing points. Obviously, some errors are introduced by the finite number of original samples per laser signal fringe. For the example given, the interpolated zero-crossing points are systematically late for the positive-going crossing and too early for the negative-going crossing because of the location in the cycle of the original samples. For the solar signal, the linear interpolator introduces errors when the interpolated zero crossing point is near a local maximum or minimum, but overall, the technique performs well. The number of original samples per laser signal fringes shown in Figure 3 is the minimum that can still result in acceptable performance. It is highly desirable to have more.

The interferograms in Figure 3 in their entirety consist of 512 samples. At 20 msec per sample, the data collection activity required about 15.6 seconds. For the same data set, Figure 4 is a graph of the time interval between consecutive interpolated zero-crossings as a function of the elapsed time since the start of data collection. Only the first four seconds of the data set is shown so that the rotation of the plate by the heated bar can be looked at in detail. The main characteristics of the bar's performance based upon this example and other tests are as follows. First, the heating and expansion is linear with elapsed time. That is, there is no apparent change in the average zero-crossing time interval during the course of a 512-element sampling and data collection process. Secondly, the small number of original samples per laser signal fringe introduces an oscillation as mentioned before. As seen from the overall data set's mean time interval and one standard deviation from that mean, this oscillation is consistent throughout the 15.6 seconds of data collection. Between three and four seconds of elapsed time, a small shift occurs that may be due to inhomogeneities in the heat transfer process through the bar, air flow modifications to the heating, or from various other reasons. The software controlling the A/D conversion has been written to enable the operator to scan the data to detect errant data in either the laser reference or solar signal and to replace them with reasonable values before proceeding with the data processing. Also, the average separation between zero-crossings and the standard deviation of the separations are computed and displayed after each data set is collected. The operator can elect to proceed with the processing if the deviation is small compared to the mean or discard the data if it appears that the data collection was disrupted in some way.

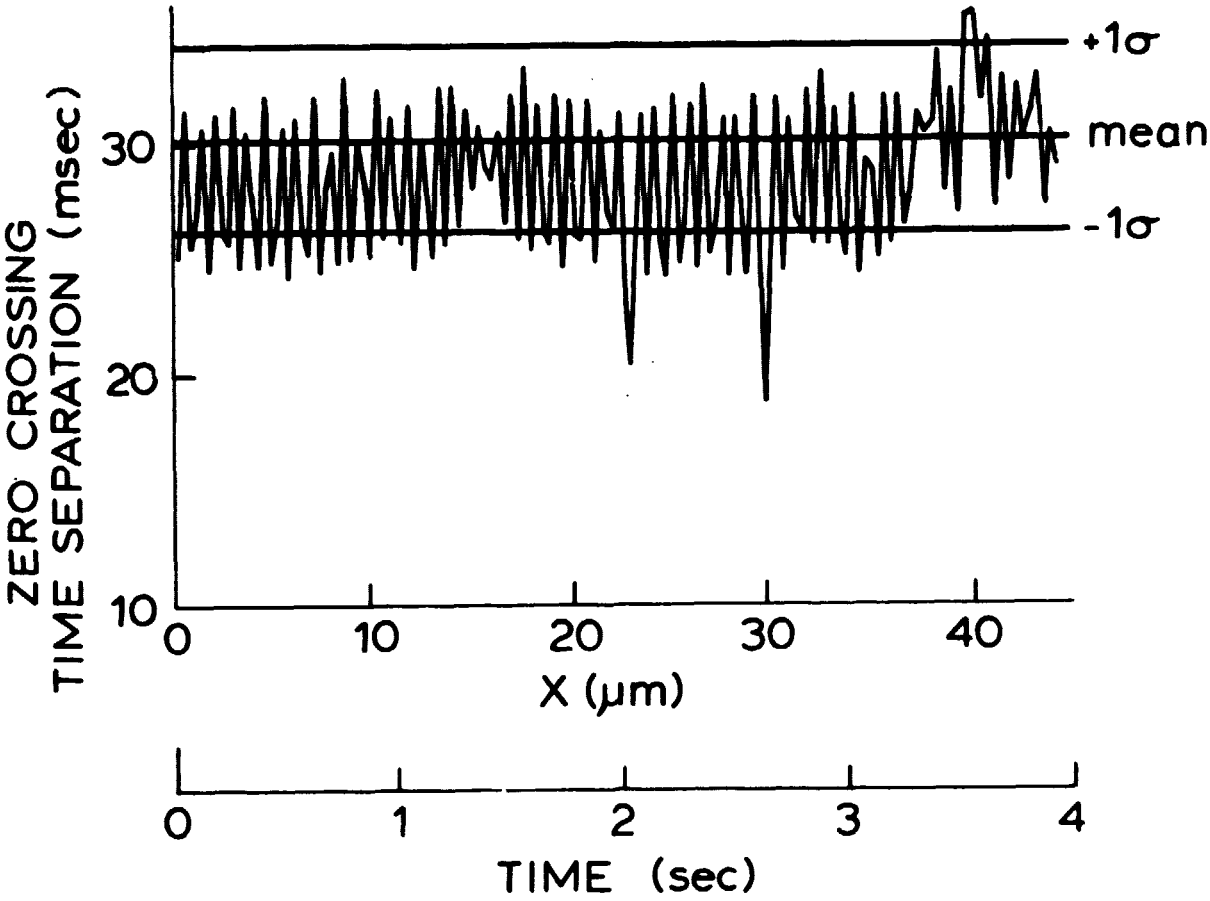

Figure 4. The variation of the time spacing between computed constant path difference samples for the first four seconds of elapsed time of a data collection procedure. The lines indicating the mean and one standard deviation bounds about the mean are computed for the entire 15.6 seconds of data collection.

The complete solar interferogram for this particular data set is shown in Figure 5. There is an asymmetric component in $\gamma(x)$ which justifies the use of the two-sided FFT as discussed earlier. The algorithm presently in use was obtained from Lloyd et al. (1980) at the University of Utah. It is coded in RT-11 V3B Fortran and is used in this system's DEC LSI-11 microcomputer. Presently the computer is equipped with 32K words of random access memory, floating point arithmetic, and an extended instruction set. All of the data presented in the following section has been processed using this FFT and an apodization function given by the following formula.

$$W\left(\frac{x}{x_T}\right) = \begin{cases} \left[1 - \left(\frac{x}{x_T}\right)^2\right]^2, & |x| \leq x_T \\ 0, & |x| > x_T \end{cases} \qquad (14)$$

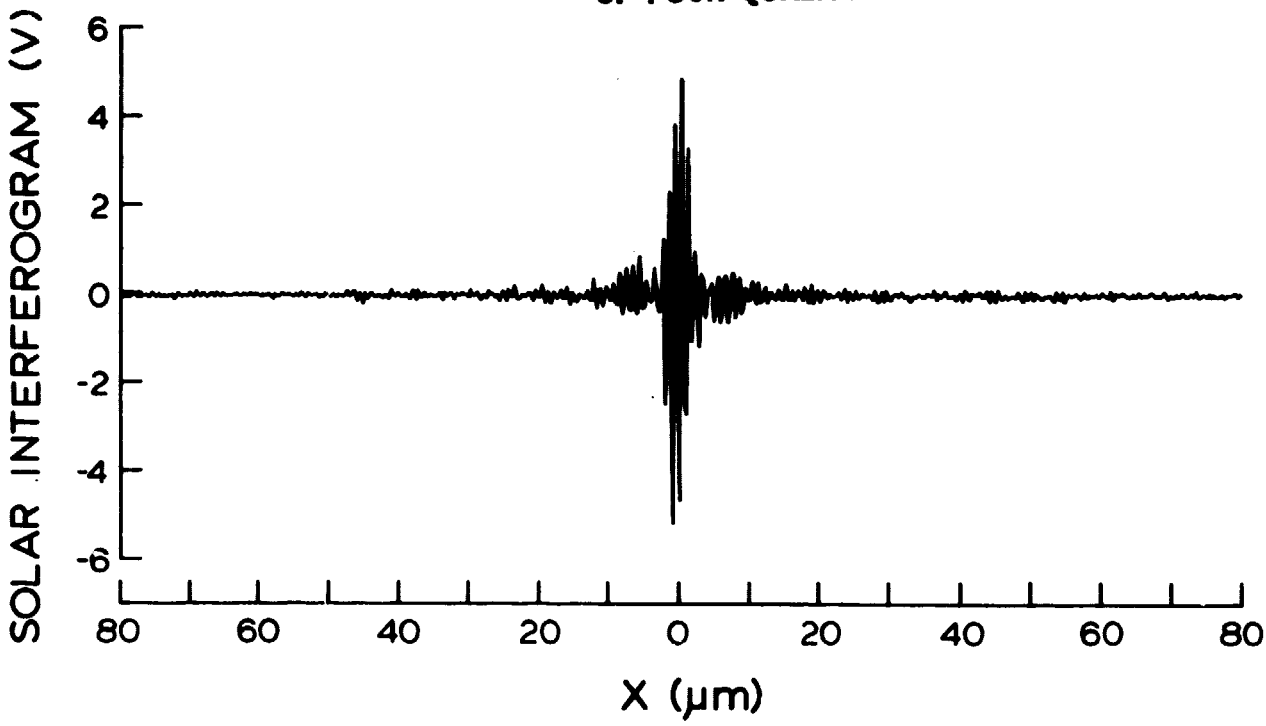

Figure 5. A 512 sample solar interferogram produced by the Wallops interferometric spectrometer.

As discussed in Chamberlain (1979), this function is effective at minimizing the effects of truncating the integral in the inverse relationship to (6). In the wavenumber domain, the transform of (14), known as the apodized spectral window, has a wide central lobe and hardly perceptible side lobes which makes it effective for routine spectroscopy where high resolution is not of paramount importance.

APPLICATIONS

Because the interferometric spectrometer is a proven instrument in the infrared, the initial spectral measurements with the prototype FTS were selected to be near the high wavelength cut-off of the photodiode at about 11,000Å. A glass filter was used to block the solar flux at wavelengths below about 6000Å. In the wavenumber domain, σ_{max} was set at 15,802 cm^{-1}, or .633 μm. From (7), (8), and (9), the path difference resolution is .3164 μm, the total path difference is 161.9968 μm, and the wavenumber resolution is 61.73 cm^{-1} for N = 512 samples.

Within the spectral region bounded by 15,802 cm^{-1} and 9000 cm^{-1}, there are several relatively prominent absorption bands from the atmosphere. Foremost of these are the "a" water vapor band (13,514-14,286 cm^{-1}), a molecular oxygen band (12,984-13,236 cm^{-1}), the "0.8 μm" water vapor band (11,905-12,658 cm^{-1}), and the "$\rho\sigma\tau$" water vapor band (9,700--11,500 cm^{-1}). The current state of knowledge concerning usable simple expressions for the atmospheric transmission in these water vapor bands can be found in a recent paper by Koepke and Quenzel (1978). Preliminary results using this FTS system are shown in Figure 6a. Spectra taken on March 9, 1982 at three different air mass values are displayed. All are normalized to their peaks, and the locations of the three water vapor bands and the O_2 band are indicated as well. For higher values of air mass, the transmission is reduced. This is most apparent for the "$\rho\sigma\tau$" band. In Figure 6b, the differences between the 1229 EST and 1430 EST spectra are graphed along with the difference between the 1229 EST and 1532 EST spectra. Again, the increased absorption for the latter comparison is obvious. Additionally, there appears to be a skewing of the spectral shape towards longer wavelengths (lower wavenumbers) for increases in air mass. In Figure 6b, this is evident as a tilt of the differences towards negative values at low wavenumbers. In the ultraviolet this behavior is expected because of molecular, or Rayleigh, scattering. In the near-infrared, it may be due to aerosol scattering. Frequently (e.g., Mecherikunnel, 1980), the effect of aerosols is modelled as

$$I = I_0 \omega e^{-\beta\lambda^{-\alpha}\mu} \tag{15}$$

where ω is the term representing the effect of all other atmospheric processes on the extraterrestrial flux I_0, and β and α are the Angstrom turbidity coefficients (Angstrom, 1951) used to characterize the aerosol's attenuation properties and λ is the wavelength in microns; μ is the air mass. For large particles, m can have the value of .5. If only the air mass variation of the aerosol term in (15) is allowed to vary, then

$$R(\lambda) = e^{-\beta\lambda^{-\alpha}1.35} \Big/ e^{-\beta\lambda^{-\alpha}2.15}$$

can be computed using the air mass values for 1229 EST and 1532 EST on March 9, 1982. Using the values $\beta = .17$ and $\alpha = 2.0$ which are typical of a turbid atmosphere with a small proportion of large particles (Mecherikunnel, 1980), the change in $R(\lambda)$ (normalized to $R(\lambda = .8\ \mu m)$) as a function of λ can be calculated and is plotted in Figure 6b. This curve is quite similar to the tilt observed in the measured spectrum as the air mass rose from 1.35 to 2.15. The measurement site is less than a mile from the Atlantic Ocean and on March 9, 1982, a strong southerly wind was blowing from the ocean to the land. There was a noticeable haze when observing the sky near the sun's location.

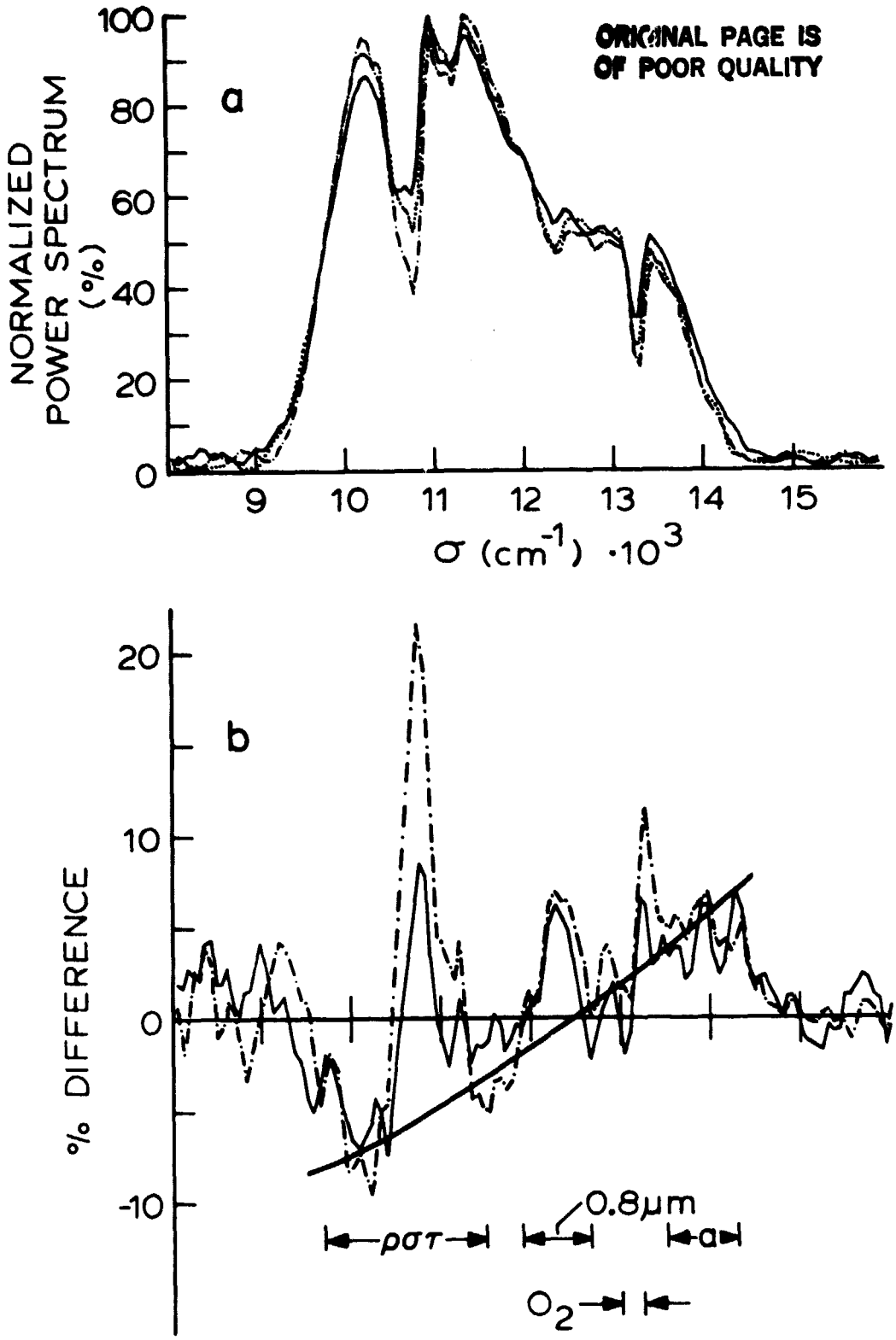

Figure 6. a) Three computed and normalized solar spectra collected March 9, 1982. Air mass values: ——, 1.35; - - -, 1.65; —·—, 2.15. b) Percentage differences between pairs of spectra in a): ——, 1.35 and 1.65; —·—, 1.35 and 2.15.

This is not intended to quantitatively describe the aerosol content of the atmosphere on the measurement date, but simply to demonstrate that the observed skewing of the measured spectra is consistent with the kind of effect that could be expected for a turbid atmosphere.

Figure 7 contrasts two spectra measured on March 8 and 9 at about 1230 EST. The visibility conditions were nearly identical. Because these data were collected at about the same air mass value, the differences observed must be due to changing amounts of the atmospheric constituents. Figure 7 isolates the "$\rho\sigma\tau$" water vapor band and a significant change from March 8 to March 9 can be seen indicating that substantially more vapor was present on the second day. Precipitable water can be defined as

$$W \triangleq \int_0^\infty \rho_v \, dz = \frac{1}{g} \int_{P_o}^0 q \, dp \qquad (17)$$

where ρ_v is the water vapor density, P_o is the surface pressure, q is the specific humidity, and g is the acceleration due to gravity. Rawinsondes are routinely launched at Wallops Island. The data were obtained from the 1200 GMT and 2400 GMT releases on March 8 and 9 and used in equation (17) to compute the precipitable water amounts. The results are tabulated below. Over twice as much water was in the atmosphere on March 9 than on March 8. The difference observed in the spectra can therefore be attributed to increased absorption by water vapor.

TABLE I. PRECIPITABLE WATER AMOUNTS AT WALLOPS ISLAND ON MARCH 8 AND 9, 1982

Date	Eastern Standard Time	Precipitable Water (mm)
3/8	0700	7.3
3/8	1900	4.0
3/9	0700	11.1
3/9	1900	12.2

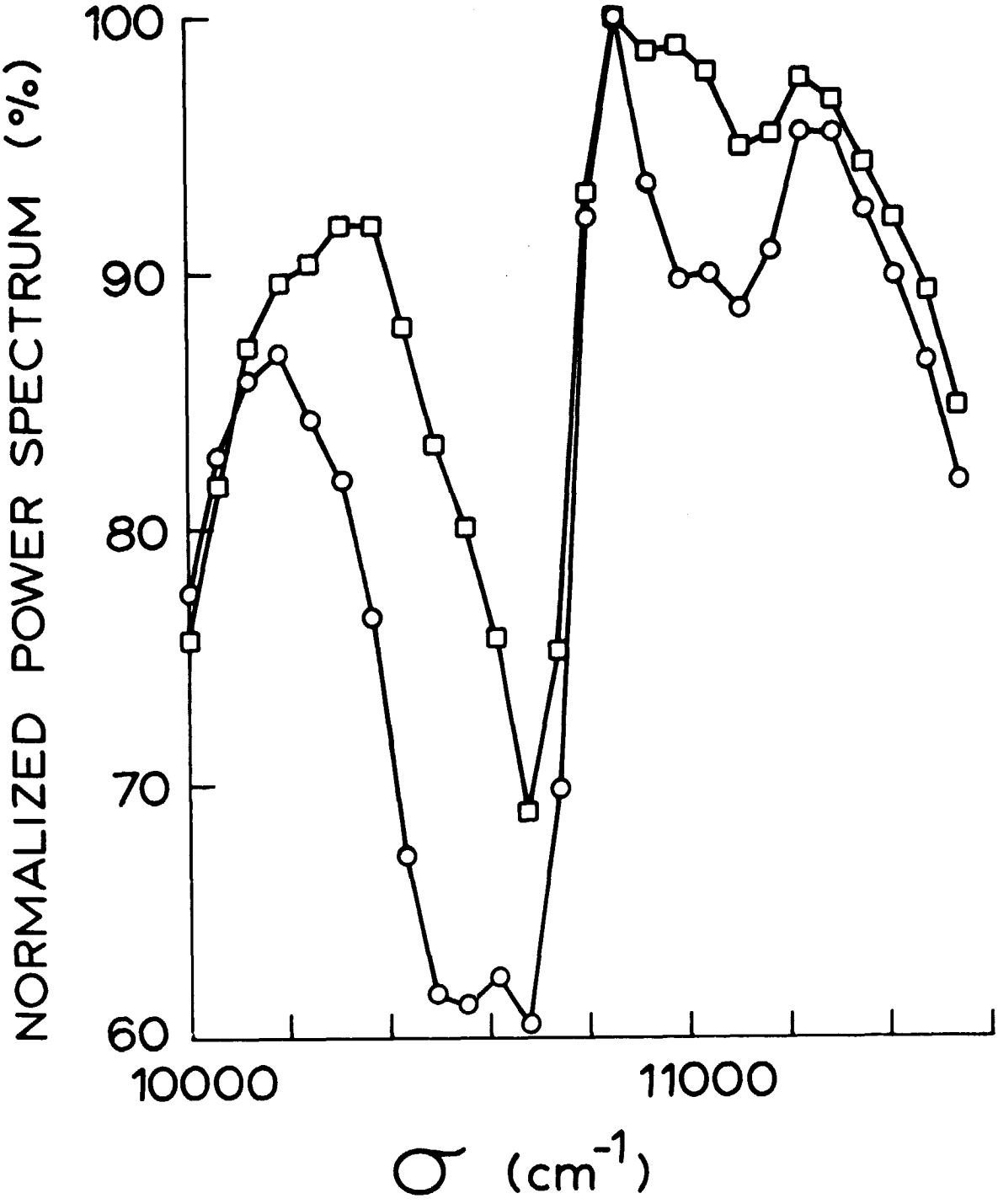

Figure 7. Normalized spectra in vicinity of "ρστ" band produced at an air mass value of 1.35 on March 8, 1982 (□) and March 9, 1982 (○).

CONCLUDING REMARKS

The prototype FTS system in use at Wallops Island, Virginia, has been described and preliminary results have been shown which demonstrate that the spectra produced by the system are consistent with the expected influences of the atmosphere on the direct solar flux. The use of the spectra to quantitatively deduce the amount of a particular gaseous absorber present in the atmospheric column or the amount and type of aerosol scatterer present has not been exploited. Various system improvements are necessary before this step can be realistically taken. Until now, the emphasis has been on the design of the optical system and the proof of the viability of the concept for making atmospheric measurements. For its full utility to be reached, the following improvements are seen as necessary. A broad-banded calibrated lamp source, if incorporated into the system, would make possible the determination of the absolute strength of the solar flux reaching the surface. In order for the FTS system to be practical in the near-ultraviolet, the rotation of the plate must be under better control. With a piezoelectric device as the source of movement, the rotation could be put under computer control and multiple sets of raw data could be collected, registered, and averaged to reduce the effect of various noises on the results. Finally, to achieve higher resolution, more samples per data set must be collected. This will require more core storage in the computer and the addition of a graphics capability to assist in quality control, display, and analysis functions. With these additions and improvements, a state-of-the-art instrument for making high resolution, absolute measurements of the near-infrared, visible, and near-ultraviolet portions of the solar spectrum at the ground will be available for a wide variety of scientific investigations.

ACKNOWLEDGMENTS

The authors want to express their gratitude to Dr. Lindsay Lloyd and his colleagues at the University of Utah for the FFT algorithm and for several helpful discussions of the FTS technique. Also, we wish to thank G. Hayne, A. Holland, J. Riley, and C. Vaughn of Wallops for their suggestions and comments.

REFERENCES

1. Angstrom, A., 1951, "Actinometric Measurements," Compendium of Meteorology, American Meteorological Society, Boston, MA, pp. 50-57.
2. Baker, D., A. Steed, and A. T. Stair, Jr., 1981, "Development of Infrared Interferometry for Upper Atmospheric Emission Studies," Applied Optics, Vol. 20, No. 10, pp. 1734-1746.
3. Brewer, A. W., 1973, "A Replacement for the Dobson Spectrophotometer," PAGEOPH, Vol. 106-108, pp. 919-927.
4. Brewer, A. W. and J. B. Kerr, 1973, "Total Ozone Measurements in Cloudy Weather," PAGEOPH, Vol. 106-108, pp. 937-938.
5. Brigham, E. O., 1974, The Fast Fourier Transform, Prentice Hall, New York.
6. Chamberlain, J., 1979, The Principles of Interferometric Spectroscopy, John Wiley and Sons, New York.
7. Dobson, G. M. B., 1931, "A Photoelectric Spectrophotometer for Measuring the Amount of Atmospheric Ozone," Proc. Phys. Soc., Vol. 43, pp. 324-339.
8. Elsworth, Y., J. F. James, and R. S. Sternberg, 1974, "A Field Compensated Interference Spectrometer for the Visible Region: The Optical Design," J. Physics E. Scientific Instruments, Vol. 7, pp. 813-816.
9. Elsworth, Y., A. R. Taylor and J. F. James, 1980, "A Field Compensated Interference Spectrometer for Spectroscopy of the Night Airglow in the Visible Region," Proc. R. Soc. London, A, Vol. 369, pp. 335-349.
10. Garrison, L. M., D. D. Doda and A. E. S. Green, 1979, "Total Ozone Determination by Spectroradiometry in the Middle Ultraviolet," Applied Optics, Vol. 18, No. 6, pp. 850-855.
11. Klein, M. V., 1970, Optics, John Wiley and Sons, New York.
12. Koepke, P. and H. Quenzel, 1978, "Water Vapor: Spectral Transmission at Wavelengths Between 0.7 μm and 1 μm," Applied Optics, Vol. 17, No. 13, pp. 2114-2118.
13. Lloyd, L. B., S. M. Riseman, R. K. Burnham, E. M. Eyring and M. M. Farrow, 1980, "Fourier Transform Photoacoustic Spectrometer," Rev. Sci. Instrum., Vol. 51, No. 11, pp. 1488-1492.
14. McMahon, B. B. and E. L. Simmons, 1980, "Ground-Based Measurements of Atmospheric NO_2 by Differential Optical Absorption," Nature, Vol. 287, pp. 710-711.
15. Mecherikunnel, A. T. and J. C. Richmond, 1980, "Spectral Distribution of Solar Radiation," NASA Technical Memorandum 82021.
16. Noxon, J. F., 1975, "Nitrogen Dioxide in the Stratosphere and Troposphere Measured by Ground-Based Absorption Spectroscopy," Science, Vol. 189, pp. 547-549.

17. Noxon, J. F., R. B. Norton and W. R. Henderson, 1978, "Observation of Atmospheric NO_3," Geophys. Res. Letters, Vol. 5, No. 8, pp. 675-678.

18. Parsons, C. L., J. C. Gerlach and M. E. Williams, 1982, "An Intercomparison of Ground-Based Total Ozone Instruments," J. Applied Meteorol., Vol 21, No. 5, pp. 88-104.

19. Platt, U. and D. Perner, 1980, "Direct Measurements of Atmospheric CH_2O, HNO_2, O_3, NO_2, and SO_2 by Differential Optical Absorption in the Near UV," J. Geophys. Res., Vol. 85, No. C12, pp. 7453-7458.

20. Platt, V., D. Perner, G. W. Harris, A. M. Winer and J. N. Pitts, Jr., 1980, "Observations of Nitrous Acid in an Urban Atmosphere by Differential Optical Absorption," Nature, Vol. 285, pp. 312-314.

21. Platt, V., D. Perner and H. W. Patz, 1979, "Simultaneous Measurement of Atmospheric CH_2O, O_3, and NO_2 by Differential Optical ABsorption," J. Geophys. Res., Vol. 84, No. C10, pp. 6329-6335.

22. Platt, V. D. Perner, A. M. Winer, G. W. Harris, and J. N. Pitts, Jr., 1980, "Detection of NO_3 in the Polluted Troposphere by Differential Optical Absorption," Geophys. Res. Letters, Vol. 7, No. 1, pp. 89-92.

23. Sternberg, R. S. and J. F. James, 1964, "A New Type of Michelson Interference Spectrometer," J. Sci. Instrum., Vol. 41, pp. 225-226.

24. Vanasse, G. A., ed., 1977, Spectrometric Techniques, Vol. I, Academic Press, New York.

25. Vanasse, G. A., ed., 1981, Spectrometric Techniques, Vol. II, Academic Press, New York.

26. Vanasse, B. A., A. T. Stair, Jr. and D. J. Baker, eds., 1971, Proceedings, Aspen International Conference on Fourier Spectroscopy, 1970, AFCRL-71-0019, 114, Bedford, MA.